# A Carrier Protein Strategy Yields the Structure of Dalbavancin

Nicoleta J. Economou, Virginie Nahoum,[†] Stephen D. Weeks,[‡] Kimberly C. Grasty, Isaac J. Zentner, Tracy M. Townsend,[§] Mohammad W. Bhuiya,[⊥] Simon Cocklin, and Patrick J. Loll*

Department of Biochemistry and Molecular Biology, Drexel University College of Medicine, Philadelphia, Pennsylvania 19102, United States

Ⓢ Supporting Information

ABSTRACT: Many large natural product antibiotics act by specifically binding and sequestering target molecules found on bacterial cells. We have developed a new strategy to expedite the structural analysis of such antibiotic−target complexes, in which we covalently link the target molecules to carrier proteins, and then crystallize the entire carrier−target−antibiotic complex. Using native chemical ligation, we have linked the Lys-D-Ala-D-Ala binding epitope for glycopeptide antibiotics to three different carrier proteins. We show that recognition of this peptide by multiple antibiotics is not compromised by the presence of the carrier protein partner, and use this approach to determine the first-ever crystal structure for the new therapeutic dalbavancin. We also report the first crystal structure of an asymmetric ristocetin antibiotic dimer, as well as the structure of vancomycin bound to a carrier−target fusion. The dalbavancin structure reveals an antibiotic molecule that has closed around its binding partner; it also suggests mechanisms by which the drug can enhance its half-life by binding to serum proteins, and be targeted to bacterial membranes. Notably, the carrier protein approach is not limited to peptide ligands such as Lys-D-Ala-D-Ala, but is applicable to a diverse range of targets. This strategy is likely to yield structural insights that accelerate new therapeutic development.
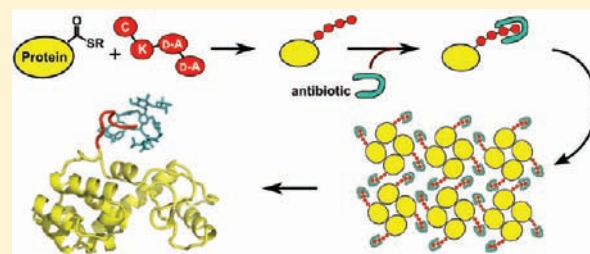
■ INTRODUCTION

Antibiotic-resistant bacterial pathogens are spreading rapidly in communities and hospitals worldwide, with concomitant increases in morbidity and mortality. Among the most infamous of these pathogens is methicillin-resistant *Staphylococcus aureus* (MRSA), which poses a particular clinical challenge due to its multidrug resistance.[1] Such infections are commonly treated with glycopeptide antibiotics, e.g. vancomycin, as "last resort" drugs. However, decades of vancomycin use have engendered resistance in many common pathogens, and vancomycin resistance has now been observed in MRSA.[2] In response, second-generation glycopeptide antibiotics are being developed, including the semisynthetic molecule dalbavancin.[3−6] Unfortunately, resistance will likely emerge to these second-generation antibiotics as well, and therefore proactive design and development of additional new antibacterials is necessary.

One promising route to new antimicrobial agents is to modify scaffolds derived from large natural products. Many such molecules are being used either as drugs or as templates for drug development, including vancomycin and other glycopeptide antibotics, nisin, bacitracin, and ramoplanin.[3,7−10]

These molecules recognize and sequester nonprotein targets on bacterial cells, such as lipids and cell wall components; since these targets are not encoded in the bacterial chromosome, there is no direct link between genomic mutations and the structure of the target molecule. As a result, resistance should develop more slowly against such drugs than against small molecules that are directed against enzymes, ribosomes, and other genetically encoded targets.

Although total syntheses have been achieved for many large natural product antibiotics,[11−14] the complexity of these molecules makes such syntheses arduous. Hence, it is challenging to optimize activity via normal medicinal chemistry approaches, requiring as they do the synthesis and testing of hundreds of variants. For such difficult molecules, a structural understanding of how they recognize their bacterial targets can prove invaluable, by directing the medicinal chemistry efforts in the most fruitful directions. However, detailed structural information is lacking for many complexes of large natural product antibiotics with their targets.

Crystallography is an excellent tool for determining structures of antibiotic−target complexes, but it is not without challenges. Producing suitable crystals can be difficult, and even when crystals are available, standard approaches to the crystallographic phase problem are not always applicable to "large small molecules" such as large natural product antibiotics; these methods either require crystals that diffract to atomic resolution, or heavy-atom or anomalous-scattering derivatives that are challenging to prepare. To address these issues, we have covalently linked an antibiotic binding epitope to a carrier protein. Carrier proteins have been successfully used as crystallization aids for many peptides and proteins.[15−17] Our chimeric carrier protein-epitope constructs promote crystallization by providing additional surface for crystal contacts and by enhancing the solubility of the antibiotic−target complex.

Additionally, the presence of the carrier protein enables facile phase determination via molecular replacement or multi-wavelength anomalous dispersion methods.

We show here that this approach is generally useful for determining structures of glycopeptide antibiotic–target complexes; in particular, it has allowed us to determine the first crystal structure for a dalbavancin–target complex, as well as the first asymmetric ristocetin–target complex. Importantly, we anticipate that this carrier protein strategy will not be limited to glycopeptide antibiotics, but will prove applicable to other antibiotic–target complexes as well. As such, it is likely to accelerate the development of novel antimicrobial therapeutics.

■ EXPERIMENTAL SECTION

Antibiotics and Vectors. Ristomycin monosulfate and vancomycin hydrochloride were purchased from Sigma-Aldrich. Dalbavancin was obtained from Biosearch Italia. The T4 lysozyme wt* gene was kindly provided by Dr. Wayne Hubbell, UCLA.[18]

Construct Preparation. Ligation-independent cloning (LIC)[19,20] was used to produce the ubiquitin$_{1-75}$- and MBP-Ala$_5$-intein vectors, and the T4 lysozyme wt*-intein vector was generated with sequence- and ligation-independent cloning (SLIC);[21] primers are given in Table S1 (Supporting Information). The lysozyme L164A mutation was constructed using the QuickChange site-directed mutagenesis kit (Stratagene). Nucleotide sequencing (Genewiz, South Plainfield, NJ) was used to verify the identity of each construct. All constructs were expressed in Rosetta2(DE3) cells (Novagen) in ZYP-5052 auto-inducing media, as described by Studier[22] with minor modifications. Cells were harvested by centrifugation, washed in deionized water, and stored at −80 °C.

Carrier protein-intein fusions were purified from cell lysates by immobilized-metal affinity chromatography. Carrier protein α-thioesters were subsequently generated by inducing intein self-cleavage with overnight incubation in 500 mM MESNA at room temperature. A second round of immobilized-metal affinity chromatography served to isolate pure carrier protein thioesters, which were concentrated to >60 mg/mL for T4 lysozyme and MBP and >25 mg/mL for ubiquitin.

Synthetic peptides were covalently linked to protein carriers using native protein ligation essentially as described.[23] Briefly, the freshly prepared carrier protein α-thioester was incubated for two days at room temperature in 0.1 M HEPES pH 8, 500 mM NaCl, 500 mM MESNA, and a 2- to 10-fold molar excess of synthetic Cys-Lys-D-Ala-D-Ala (obtained from either Anaspec or Biomatik).

Two different approaches were used to separate fused carrier protein–peptide products from unreacted species. For T4 lysozyme and MBP, native protein ligation products were reduced, desalted thoroughly, and isolated using a thiol Sepharose column, after which the cysteine residues were alkylated using a 10-fold molar excess of iodoacetic acid.[24] For the ubiquitin constructs, the desired protein ligation product was isolated using a cation exchange column, alkylated with iodoacetate, and further purified using another pass over the cation exchange column. Masses of the final, purified protein–peptide fusions were verified by mass spectrometry (NIH/NCRR Mass Spectrometry Resource, Washington University). Additional details of expression and purification are given in the Supporting Information.

Fluorescence Assay of Carrier Protein–Peptide Ligation. Samples were reduced with 5−10 mM TCEP and then passed twice over a Zeba Desalting Spin Column (Thermo Scientific) equilibrated in 20 mM HEPES pH 7, 150 mM NaCl, 10 mM EDTA. Protein concentration was measured using absorbance at 280 nm, and a large molar excess (at least 25-fold) of fluorescein-5-maleimide (Thermo Scientific) was added to the protein and incubated for 2 h at room temperature in the dark. Samples were then analyzed by reducing SDS-PAGE. Gels were fixed for 15 min in 25% isopropanol, 10% acetic acid, scanned with a STORM840 fluorescence scanner, and then stained with Coomassie Brilliant Blue.

Crystallization. The Qiagen Classic, Classic II, PEG, and PEG II Suites and the Hampton Research additive screen were used for initial crystallization screening and optimization. Final optimization of crystallization conditions was performed using hanging drop vapor diffusion in 24-well plates. All crystallization experiments were carried out at 18 °C. The T4 lysozyme−vancomycin complex was crystallized using a protein concentration of 10 mg/mL and a protein−antibiotic mole ratio of 1:1; the reservoir buffer contained 0.1 M Tris pH 8.5, 0.2 M ammonium phosphate, and 35% v/v MPD. The MBP−ristocetin complex was crystallized using a protein concentration of 10 mg/mL, a protein−antibiotic mole ratio of 1:2, and including 1 mM maltose in the protein solution; the reservoir buffer contained 5% isopropanol and 2 M ammonium sulfate. The ubiquitin−dalbavancin complex was crystallized using a protein concentration of 15 mg/mL and a protein−antibiotic mole ratio of 1:1; the reservoir buffer contained 24% PEG3350, 0.2 M ammonium tartrate, and 15 mM CYMAL-7. Prior to data collection, crystals were harvested in nylon loops, treated with cryoprotectant, and flash-cooled in liquid nitrogen. FOMBLIN Y oil was used as the cryoprotectant for T4 lysozyme−vancomycin and ubiquitin−dalbavancin, while reservoir buffer plus 22% v/v glycerol was used for MBP-ristocetin.

Structure Determination and Validation. High-resolution data sets were collected at beamline X6A of the National Synchrotron Light Source. Crystals were maintained at 93 K during data collection. Data were processed using XDS.[25] Data processing statistics are shown in Table S2 (Supporting Information). Phases were determined by molecular replacement in MOLREP[26] using the coordinates of 2LZM, 1ANF, and 3ANJ as probes for T4 lysozyme, MBP, and ubiquitin, respectively. Structure refinement was carried out using Phenix (version 1.6.2−432)[27] and Coot.[28] Refinement statistics are shown in Table S2. Stereochemical libraries for the antibiotics were generated using PRODRG[29] and HICUP.[30] Ramachandran statistics for the proteins were calculated with MOLPROBITY.[31] For the T4 lysozyme structure, 100% of the residues fall within the most favored region of the Ramachandran plot; for MBP, 98.7% of residues fall in the most favored region, and the remainder fall in the additionally allowed region; for ubiquitin, 100% of the residues fall within the most favored region. Atomic coordinates and structure factors for the T4 lysozyme−vancomycin, MBP−ristocetin, and ubiquitin−dalbavancin complexes have been deposited in the Protein Data Bank with accession codes 3RUN, 3RUM, and 3RUL, respectively. Structure figures were generated using PyMOL 0.99.rc6.[32]

Surface Plasmon Resonance (SPR). For the carrier protein−peptide fusions, ProteOn GLC sensor chips were preconditioned and then activated with a mixture of 1-ethyl-3-(3-dimethylaminopropyl carbodiimide hydrochloride) and sulfo-N-hydroxysuccinimide. Immediately after chip activation, the three protein−peptide fusions were injected across ligand flow channels for 5 min at a flow rate of 30 μL min^{-1}. The unfused, thioester forms of T4 lysozyme wt* L164A and MBP-Ala$_5$ and the ubiquitin D77 mutant were included as control surfaces. Excess active ester groups on the sensor surface were capped with ethanolamine-HCl (pH 8.5). For the free peptide Cys-Lys-D-Ala-D-Ala, ProteOn GLH sensor chips were preconditioned and activated with a mixture of 1-ethyl-3-(3-dimethylaminopropyl carbodiimide hydrochloride) and sulfo-N-hydroxysuccinimide. Next, they were immediately reacted for 3 min with 3,3′-N-[ε-maleimido-caproic acid] hydrazide (trifluoroacetic acid salt, Thermo Scientific) in 10 mM sodium borate pH 8.5, 1 M NaCl. Excess active ester groups on the sensor surface were capped with ethanolamine−HCl (pH 8.5), and then 0.01 M free peptide (in 10 mM HEPES pH 7) was injected across the ligand flow channels for 1 min at a flow rate of 30 μL min^{-1}. Finally, excess maleimide groups were reacted for 2 min with 50 mM cysteine in 0.1 M sodium acetate pH 4, 1 M NaCl. A scrambled peptide (Cys-Ala-Lys-Ala) was used as a control surface. Antibiotics were injected over the control and target ligand surfaces at a flow rate of 100 μL min^{-1}, for a 2 min association phase followed by a 3−10 min dissociation phase at 25 °C using the "one-shot kinetics" functionality of the ProteOn.[33] Data were analyzed using the ProteOn Manager Software version 3.0 (Bio-Rad). The responses of buffer injections and responses from the reference flow cell were subtracted to account for injection artifacts and nonspecific binding. Equilibrium dissociation constants (K_d) were obtained by fitting equilibrium

4638

dx.doi.org/10.1021/ja208755j | J. Am. Chem. Soc. 2012, 134, 4637−4645

Table 1. Binding Constants for Substrate Recognition by Glycopeptide Antibiotics

	K_d values from the current work (μM)				
antibiotic	T4 lysozyme fusion	MBP fusion	ubiquitin fusion	free peptide	previously published K_d values (μM)
vancomycin	3.6 ± 0.7	4.8 ± 0.1	3.6 ± 0.2	4.16 ± 0.52	0.67,[41] 0.7,[42] 1.2[a], 3.3[44]
ristocetin	2.8 ± 0.2	1.7 ± 0.3	2.0 ± 0.3	2.42 ± 0.68	1.67,[45] 0.158,[42] 6.52[a], 3.3[44]
dalbavancin	0.043 ± 0.002	0.13 ± 0.02	0.14 ± 0.02	0.855 ± 0.1	3.1[46]

[a]Derived from Arriaga et al.[43]

binding data using the 4-parameter equation in the ProteOn Manager software (Table 1). Binding curves and SPR sensorgrams are shown in the Supporting Information (Figures S4–S7, S12–S14).

RESULTS

Construct Design and Generation. The target of the glycopeptide antibiotics is the muramyl peptide of the bacterial cell wall, which terminates in the C-terminal sequence Lys-D-Ala-D-Ala. To test our carrier protein strategy in this system, we chose suitable carrier proteins and covalently linked them to a peptide containing this sequence, using protein ligation chemistry[34,35] (Scheme 1). As carrier proteins, we selected

Scheme 1. Generation of the Protein Carrier Construct[a]
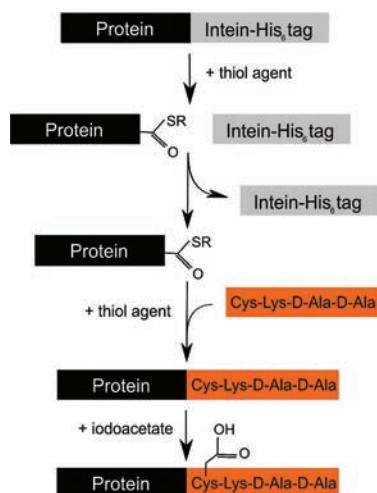
[a]Native protein ligation chemistry is used to attach the peptide ligand (orange) of the glycopeptide antibiotics to each protein carrier (black). The protein carrier is expressed as a fusion with a C-terminal intein (gray) and hexahistidine tag. After isolation of the fusion protein, addition of a thiol reagent stimulates self-cleavage, and the intein is removed via subtractive purification. Next, again in the presence of a thiol reagent, the antibiotic ligand is attached to the carrier protein via native chemical ligation. Finally, the cysteine is modified with iodoacetate, converting it to S-carboxymethyl-cysteine.

three molecules that are highly soluble, express well in *E. coli*, and by themselves produce well-diffracting crystals: T4 lysozyme, *E. coli* maltose binding protein (MBP), and ubiquitin. The carrier proteins were expressed as fusion proteins attached to a His₆-tagged *Mycobacterium xenopi* intein. In the presence of thiol agents, this intein catalyzes the cleavage of the fusion protein, releasing the carrier protein as a C-terminal α-thioester (Figures S1–S3, Supporting Information). This thioester was then attached to a synthetic Cys-Lys-D-Ala-D-Ala peptide via native protein ligation.

All of the carrier proteins chosen lacked cysteines (in the case of T4 lysozyme, we used the cysteine-free variant known as wt*[18]). Therefore, after being covalently linked to the cell wall

peptide, the carrier protein–peptide constructs all contained a single cysteine residue at the protein–peptide junction, which was used to separate fused from unfused constructs on a thiol Sepharose column (Figure S1). We also exploited the single cysteine to monitor the ligation reaction, by labeling it with a fluorescent agent (Figures S1–S3). After the ligation reaction, we modified this cysteine with iodoacetate to eliminate the possibility of disulfide bond formation, which could lead to protein heterogeneity, complicating crystallization and possibly hindering antibiotic binding.

The intein fusion protein containing T4 lysozyme was found to self-cleave at significant levels during bacterial expression. Changing the protein's C-terminal amino acid from leucine to alanine abolished this cleavage,[36] and so the L164A mutant of wt* was used for all further studies. MBP was chosen because it has previously proven useful as a fusion partner in crystallization experiments;[37] it can also adopt two stable conformations, free and maltose-bound,[38,39] increasing the probability that the construct can find molecular contacts conducive to crystal formation. We expressed MBP as MBP-Ala₅, with a C-terminal five-alanine linker designed to extend outward from the body of the protein and thus provide room for antibiotic binding. Ubiquitin was chosen because it is highly stable, and because its C-terminus naturally extends away from the globular body of the protein. We used a construct corresponding to the first 75 amino acids of ubiquitin (ubiquitin₁–₇₅), reasoning that removing the protein's C-terminal glycine residue might increase the rigidity of the C-terminal extension and improve crystallization behavior.

All three carrier proteins were produced in excellent yields as recombinant proteins in *E. coli*. Ligation of the target peptide to the carrier protein was successful in all three cases, and in each case we were able to purify to homogeneity multimilligram quantities of the carrier protein–peptide fusion (Figures S1–S3).

Validation of the Carrier Protein Approach. To confirm that the presence of the carrier protein does not disturb the antibiotic–target interactions, we tested a panel of glycopeptide antibiotics for their ability to bind to the carrier protein–peptide constructs, as well as to the peptides themselves. Two of the antibiotics (vancomycin and ristocetin) recognized all three fusion constructs with affinities similar to those with which they bind the Lys-D-Ala-D-Ala peptides themselves (Table 1 and Figures S4–S7).[40–46] The third antibiotic, dalbavancin, actually bound the fusion constructs with higher apparent affinities than the isolated peptide, suggesting that the presence of the carrier protein can enhance target binding (discussed below). In any case, the presence of the carrier protein did not disrupt antibiotic–target recognition.

We next examined whether the carrier proteins were able to facilitate the crystallographic study of glycopeptide antibiotics as intended. We tested the crystallization of two glycopeptide antibiotics, vancomycin and ristocetin, in the presence of the three carrier protein–peptide fusions. Using standard screening
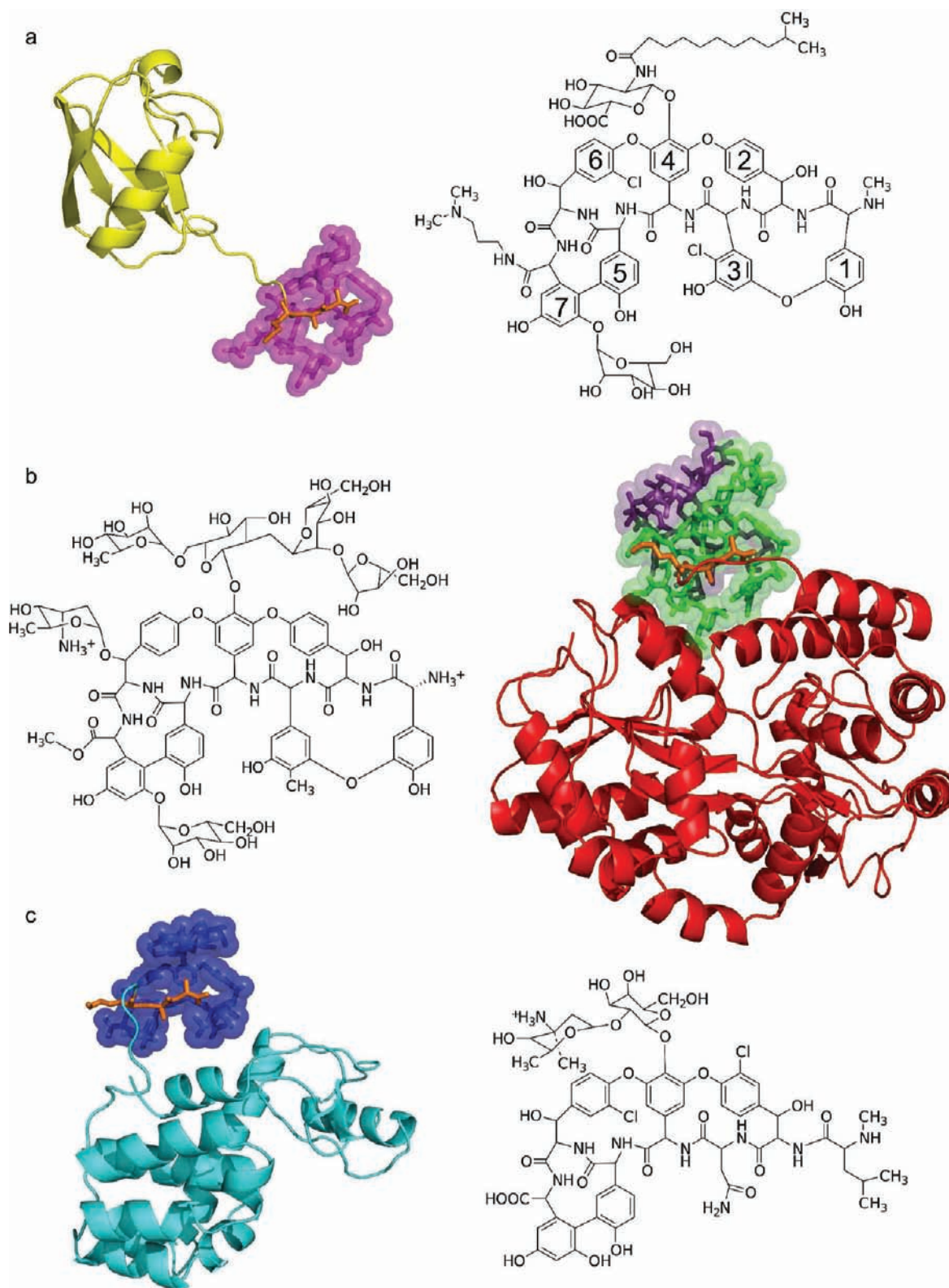
Figure 1. Structures of glycopeptide antibiotics in complex with carrier protein—peptide fusions. (a) (Left) The semisynthetic glycopeptide antibiotic dalbavancin (magenta) bound to its Lys-D-Ala-D-Ala ligand (orange), which is fused to a ubiquitin molecule (yellow). (Right) Chemical structure of dalbavancin. Glycopeptide antibiotics are typically hepta-peptides of noncanonical amino acids (illustrated in this panel by numbers 1—7), decorated by sugars. (b) (Left) Chemical structure of ristocetin. (Right) Ristocetin dimer (green and purple) bound to its Lys-D-Ala-D-Ala ligand (orange), which is fused to an MBP molecule (red). (c) (Left) Vancomycin (blue) bound to its Lys-D-Ala-D-Ala substrate (orange), which is fused to a T4 lysozyme molecule (cyan). (Right) Chemical structure of vancomycin.

approaches, we obtained well-diffracting crystals for both antibiotics, with vancomycin crystallizing in complex with T4

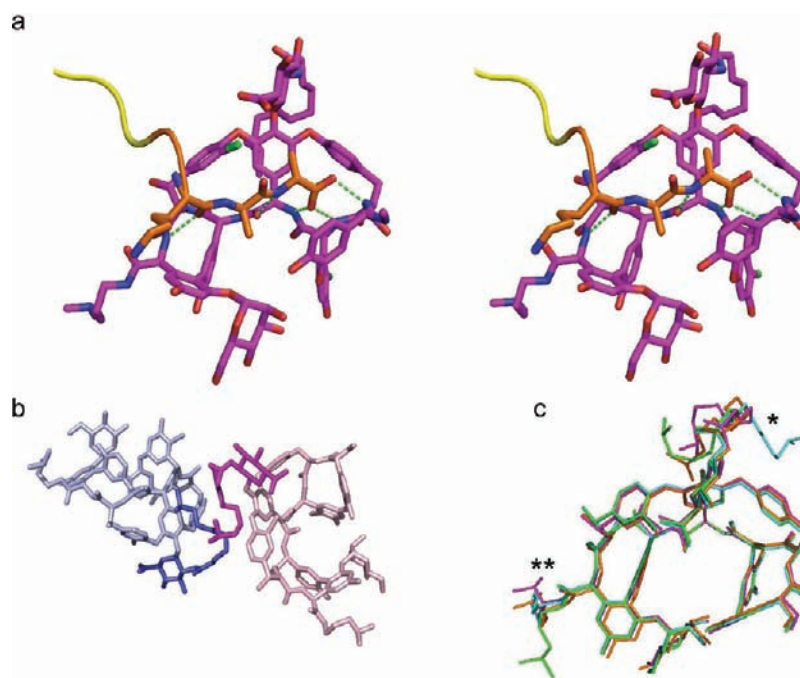lysozyme and ristocetin with MBP (Table S2, Supporting Information). The two crystal structures were readily

Figure 2. First crystal structure of dalbavancin. (a) Stereo view of dalbavancin illustrating target recognition; five signature hydrogen bonds connect the antibiotic (magenta) with its Lys-D-Ala-D-Ala target (orange). The C-terminus of the ubiquitin carrier protein is shown in yellow. (b) Two dalbavancin molecules (pink and light blue) associate loosely via their fatty acyl groups (magenta and dark blue). (c) Superposition of all four dalbavancin structures in the crystal asymmetric unit, shown in magenta, orange, cyan, and green. Conformational heterogeneity is apparent in both the fatty acyl group (marked with *) and the dimethyl-propylamine group (**). These two groups improve dalbavancin's antimicrobial activity and half-life.

determined by molecular replacement (Figure 1), giving clear electron densities for the antibiotics (Figure S10). The final refined structures revealed both antibiotics binding specifically to the Lys-D-Ala-D-Ala moiety of the fusion constructs, forming five hydrogen bonds with the ligand as previously described[47−49] (Figures 1, S8). In the vancomycin structure, the liganded vancomycin monomer lies near a crystallographic 2-fold axis and forms a back-to-back dimer with a symmetry-related copy of itself (Figure S9). The structure of the aglycon portion of this back-to-back dimer is essentially identical to those previously determined.[50,51] The positions of the sugars of the vancomycin dimer appear slightly different in this structure than in previous structures, but it is worth noting that the sugars are partially disordered in this new structure (their position on a crystallographic two-fold axis means that two different conformers are present). Thus, any such apparent differences from previous structures should be interpreted with caution. In the ristocetin-MBP structure, the configuration of the peptide-bound monomer is again identical to that seen in a previously determined structure,[48] with an rms deviation of Cα positions of 0.097 Å (Figure S8). These results provide further evidence that the presence of the carrier protein does not perturb the antibiotic structure, and show that the carrier protein strategy is both feasible and appropriate for studying the details of the molecular interactions between glycopeptide antibiotics and their targets.

Dalbavancin Structure. We next examined whether the carrier protein strategy could expedite a difficult structure determination problem, namely that of the dalbavancin antibiotic–target complex. In our hands, the complex of dalbavancin with its target peptide proved highly refractory to crystallization, and resisted structure determination even after sustained efforts. In contrast, dalbavancin crystallized readily in

the presence of the ubiquitin carrier protein–peptide fusion, and the structure was easily determined by molecular replacement, providing the first-ever crystal structure of dalbavancin (Figures 1 and 2).

Each asymmetric unit of the crystal contains two pairs of ubiquitin–dalbavancin complexes. Within each pair, the two dalbavancin molecules associate loosely back-to-back via their fatty acid moieties (Figures 2b, S11). However, the dalbavancin molecules do not form the intimate, hydrogen-bonded back-to-back dimers seen with many other glycopeptide antibiotics; this is not surprising, since the fatty acyl chain sterically blocks the close back-to-back approach of two monomers and prevents dimerization, as is also true in the structurally similar molecule teicoplanin.[52] Each dalbavancin molecule closes around its Lys-D-Ala-D-Ala target, making five hydrogen bonds with backbone oxygen and nitrogen atoms of the peptide, in addition to making van der Waals contacts with the D-alanine side chains (Figure 2a). The glucuronic acid sugar that is attached to residue 4 of the antibiotic overhangs the binding site for the cell wall peptide; it helps to bury the bound peptide, but does not make specific polar interactions with the ligand. The fatty acyl group of the antibiotic lies on the "back" of the antibiotic molecule, i.e., the side opposite the ligand binding site; the conformations of the fatty acyl chains differ between the four independent copies of the antibiotic found in the asymmetric unit, suggesting a degree of flexibility for this group (Figure 2c). Similarly, the C-terminal dimethyl-propylamine group of the antibiotic shows signs of disorder and does not interact with the ligand.

The structure of dalbavancin is significantly more closed than that of the A40926 aglycon, a closely related molecule.[53] In the dalbavancin structure, the mannose attached to amino acid 7, at one end of the molecule, packs onto the side chains of amino

acids 1 and 3 at the other end of the molecule, causing the antibiotic to wrap around the ligand. However, in the ligand-free A40926 structure, the two ends of the molecule remain considerably further apart, causing the overall configurations of dalbavancin and A40926 to diverge significantly (rmsd of Cα positions ∼0.9 Å; see Figure 3). A similar unbound-open/
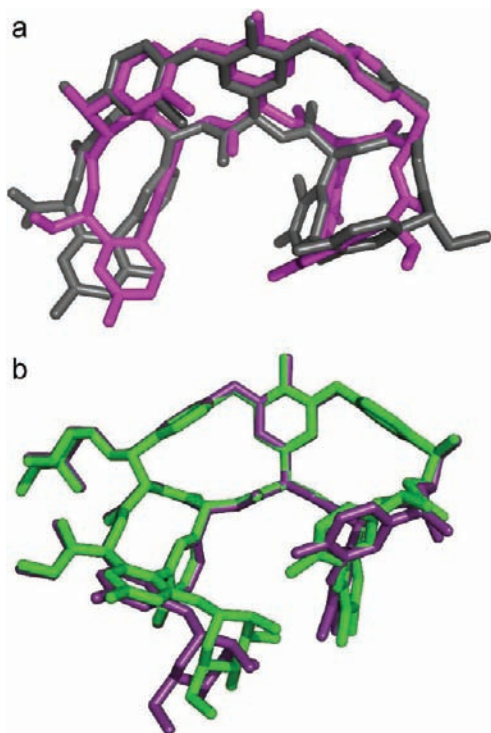

Figure 3. Comparison of the open and closed configurations of glycopeptide antibiotics. (**a**) Superposition of dalbavancin (magenta) and the A40926 aglycon (gray). (**b**) Superposition of the two ristocetin monomers. In the liganded monomer (green), closure occurs via a hydrogen bond interaction between the mannose and amino acid 1, which is not seen in the unliganded monomer (purple).

bound-closed pattern is also seen in ristocetin, suggesting that ligand binding induces closure; however, the sugars and lipids present in dalbavancin (and not found in the A40926 aglycon) might also contribute steric restraints that encourage a more closed conformation.[54]

An Asymmetric Ristocetin Dimer. Additional insights made possible by the carrier protein approach could be found in the ristocetin−MBP structure. Ristocetin dimerization is anti-cooperative with ligand binding, implying that the two binding sites within an antibiotic dimer bind ligand with nonequivalent affinities.[55] However, in previous crystallographic studies of the ristocetin−Lys-D-Ala-D-Ala complex, the two sites could not be distinguished, since the crystals contained only one monomer in the asymmetric unit, and therefore represented an average of high- and low-affinity conformations.[48] In contrast, in the new ristocetin structure derived from the carrier-protein strategy only a single ligand is bound to the antibiotic dimer, revealing which is the higher affinity site.

In the ristocetin dimer, the two peptide backbones adopt a back-to-back, antiparallel configuration, while the two tetrasaccharides pack in a parallel configuration, placing either an arabinose or a rhamnose over the ligand binding site, and thereby making the dimer asymmetric (Figure 4). In addition
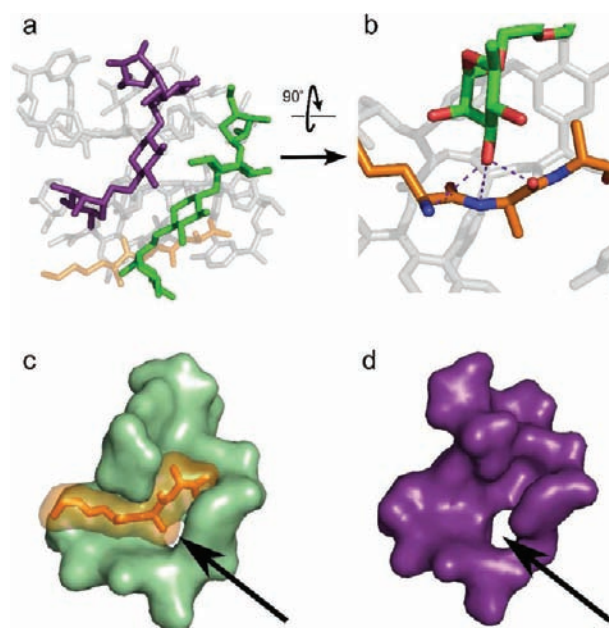

Figure 4. Structure of the asymmetric ristocetin dimer. (a) Top view of the asymmetric dimer. The tetrasaccharides of the two monomers are shown in green and purple. The ligand is shown in orange, and the two ristocetin pseudoaglycons in gray. The rhamnose molecule of the green tetrasaccharide overhangs the higher affinity (occupied) binding site. (b) The rhamnose of the liganded monomer interacts with the antibiotic target via three hydrogen bonds. This view is rotated 90° with respect to that used in panel (a). (c,d). Ligand binding causes ristocetin to close around its target. In panel (c), a surface representation is shown for the liganded ristocetin monomer (green), along with the bound ligand (orange), revealing the closure of ristocetin onto its target. In panel (d), a comparable representation is shown for the unliganded ristocetin monomer. Note how the small gap in the molecule (shown by an arrow in both panels) is smaller in the liganded monomer, as a consequence of the molecule closing around its target.

to the gross asymmetry of the tetrasaccharides, the remainder of the molecule exhibits a more subtle asymmetry, undetected in previous solution studies,[49] with the liganded and unliganded monomers adopting closed and open conformations, respectively. In the closed conformation, the mannose of amino acid 7 hydrogen-bonds with the side chain of amino acid 1, bringing the two ends of the antibiotic together to embrace the ligand in a manner similar to that seen with dalbavancin (Figure 3). This interaction does not occur in the unliganded monomer, causing it to adopt a relatively open configuration. The rms difference in Cα positions between the liganded and unliganded ristocetin monomers is 0.35 Å.

The occupied binding site is adjacent to the rhamnose sugar of the tetrasaccharide. The rhamnose forms three additional hydrogen bonds with the Lys-D-Ala-D-Ala peptide, in addition to the five hydrogen bonds made between the peptide and the aglycon portion of the antibiotic (Figure 4). The additional affinity contributed by these hydrogen bonds explains the higher affinity of this monomer. This direct structural determination of the high affinity site agrees well with a previous model proposed from solution studies.[49]

■ **DISCUSSION**

This work was motivated by the need for high-resolution structural analyses of natural product antibiotics in complex

with their targets; the resulting structural information can aid the design of novel therapeutics based on natural product scaffolds. The carrier protein strategy described in this paper was specifically designed to overcome practical barriers that can stymie such structure determination efforts. While crystallography has successfully provided structural insights into many antibiotic–ligand complexes, in some subset of the cases studied significant problems are encountered, either at the stage of generating crystals suitable for diffraction analysis, or at the stage of solving the phase problem. The former problem is by no means unique to "large small molecules" such as natural product antibiotics, but it is reasonable to expect that flexible and/or hydrophobic ligands such as peptides or lipids will complicate crystallization, as will the intrinsic low aqueous solubility of many antibiotics themselves. On the other hand, phase determination can present unique challenges for large small molecules. Methods that have been developed for experimentally phasing protein and nucleic acid structures are generally not applicable to natural products; direct phasing methods, while applicable, require crystals that diffract to extremely high resolution, which are frequently impossible to obtain. We therefore implemented the carrier protein strategy, in which an antibiotic's ligand is chemically coupled to a protein, after which the entire protein–ligand–antibiotic complex is crystallized. This approach has the potential to solve both crystallization and phasing problems: The carrier protein enhances crystallization by increasing solubility, providing additional surface area for crystal contacts, and possibly reducing conformational heterogeneity, and it provides solutions to the phase problem via molecular replacement or selenomethionine MAD phasing.

An example of the sort of molecule for which this strategy has been developed is dalbavancin, a second generation, semisynthetic glycopeptide antibiotic currently in phase III clinical trials for the treatment of MRSA and other drug-resistant Gram-positive bacterial infections. Like other glycopeptide antibiotics, dalbavancin is a heptapeptide of non-canonical amino acids, and is decorated by sugar moieties on amino acids 4, 6, and 7. It also carries a fatty acid attached to one of the sugars, and a C-terminal dimethyl-aminopropyl group. These substituents enhance the antibiotic's activity against Gram-positive bacteria, including some vancomycin-resistant enterococci and staphylococci.[56–59]

In our hands, the complex of dalbavancin with its cell-wall peptide target proved highly refractory to crystallization. Extensive screening gave only a single crystal form, which diffracted weakly and contained over 20 molecules in the asymmetric unit,[60] making it unsuitable for structure determination by either direct methods or molecular replacement. However, as we had envisioned when embarking on this project, coupling the peptide ligand to the small protein ubiquitin allowed us to crystallize the dalbavancin–target complex; subsequent structure determination by molecular replacement proved straightforward, using the known structure of ubiquitin as a probe. When we conducted similar exercises with vancomycin and ristocetin, two antibiotics of known structure, we were likewise able to generate crystals with little difficulty and easily determined the structures using molecular replacement. For this strategy to prove generally useful, it is essential that the presence of the protein partner does not perturb antibiotic–target recognition, nor alter the structure of the antibiotic itself. Using an SPR assay, we tested three different glycopeptide antibiotics for their ability to bind to three different carrier protein–target peptide fusions; in all cases we measured K_d values that are either comparable to or lower than those found in the literature, indicating that the various carrier proteins did not disrupt target recognition by the antibiotics. In a further test, we crystallized a carrier protein–target peptide fusion in complex with vancomycin, the most thoroughly characterized of the glycopeptide antibiotics. The structure thus obtained for vancomycin in complex with its Lys-D-Ala-D-Ala target shows antibiotic–peptide interactions identical with those previously identified (Figure S9); interestingly, two vancomycin molecules are seen to exploit crystallographic symmetry to form the same back-to-back dimer that is seen in all other vancomycin–ligand structures, demonstrating that the presence of the carrier protein affects neither the three-dimensional structure of the antibiotic, nor its ability to form higher order assemblies.

Previously, the only available structure of a compound related to dalbavancin was that of the unliganded A40926 aglycon, which shares the same peptide backbone as dalbavancin, but lacks the clinically important sugar and lipid substituents. Our dalbavancin structure reveals a substantially more closed conformation than that seen in the A40926 aglycon (Figure 3). Closure of the antibiotic around the ligand will induce favorable van der Waals interactions between antibiotic and target, as well as strengthening hydrogen bonds between antibiotic and target by shielding them from solvent. Dalbavancin's closed conformation is probably triggered, at least in part, by the binding of ligand to the antibiotic; however, it is also likely to reflect conformational restraints imposed by the sugars and additional groups found in the intact molecule,[54] highlighting the importance of studying the complete antibiotic structure. This would not have been possible without the carrier protein strategy.

Another example of the link between the closed conformation and ligand binding is seen in the ristocetin structure that emerged from our carrier protein work. Ristocetin is unique among the glycopeptide antibiotics insofar as ligand binding is anticooperative with dimerization.[55,61] We reasoned that this anticooperativity should make it possible to crystallize a monoliganded antibiotic dimer, allowing us to examine the structural differences that give rise to anticooperativity. However, previous attempts to crystallize the ristocetin–peptide complex yielded crystals in which the antibiotic dimer lay on a crystallographic two-fold symmetry axis, with both binding sites of the dimer perforce occupied.[48] Fusing ristocetin's ligand to a protein partner allowed us to circumvent this difficulty, affording crystals that contained the desired monoliganded dimer. Within this asymmetric dimer structure, the two monomers adopt two different conformations, not previously detected in solution studies. The ligand-free monomer adopts the open form, while the ligand-bound monomer is in the closed form (Figures 3 and 4). Although a ligand-free dalbavancin structure is not currently available, the similar open/closed difference seen between dalbavancin and the A40926 aglycon suggests that closure about the ligand might be a general feature of such molecules (which belong to the so-called group III of the glycopeptide antibiotics).[62]

Dalbavancin's fatty acyl group and C-terminal dimethyl-aminopropyl moiety are thought to enhance binding avidity at the site of bacterial cell wall biosynthesis, either by inserting into the bacterial membrane or by mediating multimerization. The structure presented here shows that the C-terminal dimethyl-propylamine group is free and flexible, suggesting

that this group would be available to bind the negative phospholipid head groups of the bacterial membrane; the relative orientation of the two groups would allow the fatty acyl chain to simultaneously insert into the bilayer. The structure also shows fatty acyl groups of different dalbavancin molecules associating, consistent with dalbavancin's propensity to multimerize.[46]

An important aspect of dalbavancin's enhanced antimicrobial activity is its long half-life in patients, thought to derive from binding to serum proteins.[63,64] Consistent with a proclivity for protein binding, dalbavancin's fatty acyl chain and the aromatic ring of amino acid 2 are packed into hydrophobic pockets on the surface of ubiquitin in our structure (Figure 5). The fatty
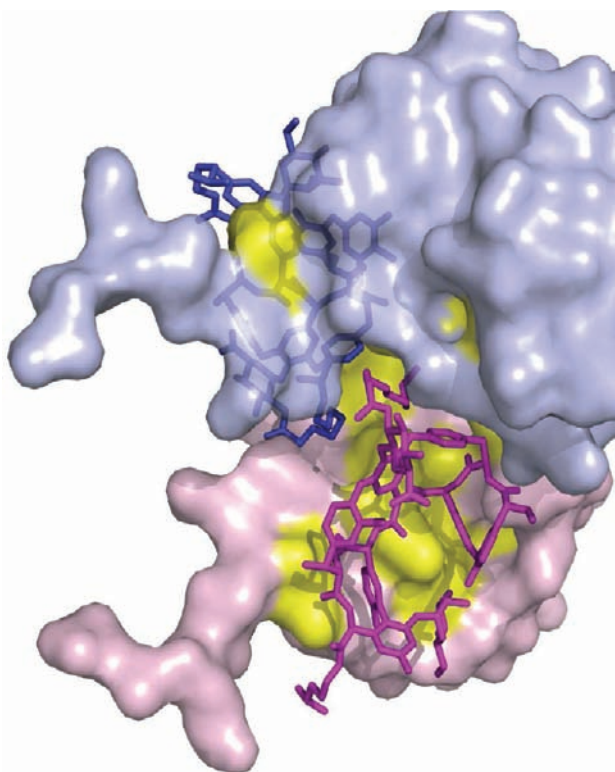

Figure 5. Dalbavancin interacts with protein surfaces. Two dalbavancin molecules (magenta and blue) interact with hydrophobic pockets (yellow) found on two adjacent ubiquitin molecules (light pink and blue).

acid chains belonging to the different copies of dalbavancin in the asymmetric unit adopt different conformers. While such flexibility might allow the drug to bind to hydrophobic patches on different serum proteins, it was undoubtedly an impediment to the crystallization of dalbavancin. However, this problem could be overcome during the carrier protein experiment, when the fatty acyl chains were immobilized by packing against hydrophobic surface patches of ubiquitin. Protein binding effects are a likely explanation for dalbavancin's higher apparent affinities for immobilized carrier protein—peptide fusions than for immobilized peptides, as well as for the subtle affinity differences seen with different carrier proteins. This may seem at odds with reports that the presence of serum albumin reduces dalbavancin's apparent affinity for muramyl peptides in a calorimetry assay,[46] but can be reconciled after recognizing that in a three-dimensional binding assay (e.g., calorimetry), protein binding can reduce the effective concentration of the

antibiotic, while in a two-dimensional assay (like SPR) binding to immobilized protein can actually increase the antibiotic's effective concentration at the sensor surface. Given that the environment of the nascent bacterial cell wall is essentially two-dimensional, and rich in protein, such nonspecific protein binding may increase the local concentration of dalbavancin and thereby drive antibiotic binding to its target sites.

CONCLUDING REMARKS

We describe a novel carrier protein strategy that has facilitated structure determination for several different "large small molecule" antibiotics in complex with their ligands. These structures include the first crystal structure of the new therapeutic dalbavancin and the first crystal structure of an asymmetric ristocetin dimer, and provide new insights into the antibiotics' mechanisms of action. The technology described herein has applications that extend beyond crystallography; we have shown that the carrier protein—target fusions provide excellent reagents for use in SPR experiments, and one can also imagine their use in binding experiments using fluorescence anisotropy. Notably, this approach is not limited to antibiotics that recognize cell-wall peptide ligands, but can also be applied to a broad range of other antibiotic targets. We therefore anticipate that this approach will accelerate structure determination of target complexes for different classes of antibiotics, thereby assisting the proactive development of next-generation antibacterial drugs.

ASSOCIATED CONTENT

S Supporting Information

Two tables, 14 figures, complete ref 27; additional details of carrier protein construct preparation and validation; crystallographic statistics; SPR sensorgrams; additional structural figures. This material is available free of charge via the Internet at http://pubs.acs.org.

AUTHOR INFORMATION

Corresponding Author
ploll@drexelmed.edu

Present Addresses
[†]Institut de Pharmacologie et de Biologie Structurale, CNRS-Université Paul Sabatier III, Toulouse, France
[‡]Laboratory of Biocrystallography, Department of Pharmaceutical Sciences, K U Leuven, Belgium
[§]GlaxoSmithKline, King of Prussia, PA, USA
[⊥]Conagen Inc., St. Louis, MO, USA

Notes
The authors declare no competing financial interest.

ACKNOWLEDGMENTS

REFERENCES

(1) French, G. L. *Int. J. Antimicrob. Agents* **2010**, *36* (Suppl 3), S3−7.
(2) Appelbaum, P. C. *Clin. Microbiol. Infect.* **2006**, *12* (Suppl 1), 16−23.

(3) Zhanel, G. G.; Calic, D.; Schweizer, F.; Zelenitsky, S.; Adam, H.; Lagace-Wiens, P. R.; Rubinstein, E.; Gin, A. S.; Hoban, D. J.; Karlowsky, J. A. *Drugs* **2010**, *70*, 859−886.

(4) Malabarba, A.; Goldstein, B. P. *J. Antimicrob. Chemother.* **2005**, *55* (Suppl2), ii15−20.

(5) Chen, A. Y.; Zervos, M. J.; Vazquez, J. A. *Int. J. Clin. Pract.* **2007**, *61*, 853−863.

(6) Bailey, J.; Summers, K. M. *Am. J. Health. Syst. Pharm.* **2008**, *65*, 599−610.

(7) Kahne, D.; Leimkuhler, C.; Lu, W.; Walsh, C. *Chem. Rev.* **2005**, *105*, 425−448.

(8) Lubelski, J.; Rink, R.; Khusainov, R.; Moll, G. N.; Kuipers, O. P. *Cell. Mol. Life Sci.* **2008**, *65*, 455−476.

(9) Ming, L. J.; Epperson, J. D. *J. Inorg. Biochem.* **2002**, *91*, 46−58.

(10) McCafferty, D. G.; Cudic, P.; Frankel, B. A.; Barkallah, S.; Kruger, R. G.; Li, W. *Biopolymers* **2002**, *66*, 261−284.

(11) Boger, D. L. *Med. Res. Rev.* **2001**, *21*, 356−381.

(12) Jiang, W.; Wanner, J.; Lee, R. J.; Bounaud, P. Y.; Boger, D. L. *J. Am. Chem. Soc.* **2003**, *125*, 1877−1887.

(13) Fukase, K.; Kitazawa, M.; Sano, A.; Shimbo, K.; Fujita, H.; Horimoto, S.; Wakamiya, T.; Shiba, T. *Tetrahedron Lett.* **1988**, *29*, 795−798.

(14) Lee, J.; Griffin, J. H.; Nicas, T. I. *J. Org. Chem.* **1996**, *61*, 3983−3986.

(15) Moon, A. F.; Mueller, G. A.; Zhong, X.; Pedersen, L. C. *Protein Sci.* **2010**, *19*, 901−913.

(16) Koide, S. *Curr. Opin. Struct. Biol.* **2009**, *19*, 449−457.

(17) Derewenda, Z. S. *Acta Crystallogr. D Biol. Crystallogr.* **2010**, *66*, 604−615.

(18) Matsumura, M.; Matthews, B. W. *Science* **1989**, *243*, 792−794.

(19) Aslanidis, C.; de Jong, P. J. *Nucleic Acids Res.* **1990**, *18*, 6069−6074.

(20) Haun, R. S.; Serventi, I. M.; Moss, J. *Biotechniques* **1992**, *13*, 515−518.

(21) Li, M. Z.; Elledge, S. J. *Nat. Methods* **2007**, *4*, 251−256.

(22) Studier, F. W. *Protein Expr. Purif.* **2005**, *41*, 207−234.

(23) Evans, T. C. Jr.; Benner, J.; Xu, M. Q. *Protein Sci.* **1998**, *7*, 2256−2264.

(24) Hermanson, G. T. *Bioconjugate techniques*, 1st ed.; Academic Press: San Diego, CA, 1996.

(25) Kabsch, W. *Acta Crystallogr. D Biol. Crystallogr.* **2010**, *66*, 125−132.

(26) Vagin, A.; Teplyakov, A. *Acta Crystallogr. D Biol. Crystallogr.* **2010**, *66*, 22−25.

(27) Adams, P. D.; et al. *Acta Crystallogr. D Biol. Crystallogr.* **2010**, *66*, 213−221.

(28) Emsley, P.; Lohkamp, B.; Scott, W. G.; Cowtan, K. *Acta Crystallogr. D Biol. Crystallogr.* **2010**, *66*, 486−501.

(29) Schuttelkopf, A. W.; van Aalten, D. M. *Acta Crystallogr. D Biol. Crystallogr.* **2004**, *60*, 1355−1363.

(30) Kleywegt, G. J.; Jones, T. A. *Acta Crystallogr. D Biol. Crystallogr.* **1998**, *54*, 1119−1131.

(31) Richardson, D. C.; Chen, V. B.; Arendall, W. B.; Headd, J. J.; Keedy, D. A.; Immormino, R. M.; Kapral, G. J.; Murray, L. W.; Richardson, J. S. *Acta Crystallogr. D Biol. Crystallogr.* **2010**, *66*, 12−21.

(32) DeLano, W. L. *The PyMOL Molecular Graphics System*, version 0.99rc6; DeLano Scientific: San Carlos, CA, 2002.

(33) Bravman, T.; Bronner, V.; Lavie, K.; Notcovich, A.; Papalia, G. A.; Myszka, D. G. *Anal. Biochem.* **2006**, *358*, 281−288.

(34) Muir, T. W. *Annu. Rev. Biochem.* **2003**, *72*, 249−289.

(35) Muralidharan, V.; Muir, T. W. *Nat. Methods* **2006**, *3*, 429−438.

(36) *Protein Expression and Analysis*, 1.0 ed.; New England Biolabs: Ipswich, 2009; pp 1−34.

(37) Smyth, D. R.; Mrozkiewicz, M. K.; McGrath, W. J.; Listwan, P.; Kobe, B. *Protein Sci.* **2003**, *12*, 1313−1322.

(38) Quiocho, F. A.; Spurlino, J. C.; Rodseth, L. E. *Structure* **1997**, *5*, 997−1015.

(39) Duan, X.; Quiocho, F. A. *Biochemistry* **2002**, *41*, 706−712.

(40) Beauregard, D. A.; Maguire, A. J.; Williams, D. H.; Reynolds, P. E. *Antimicrob. Agents Chemother.* **1997**, *41*, 2418−2423.

(41) Nieto, M.; Perkins, H. R. *Biochem. J.* **1971**, *123*, 789−803.

(42) Cooper, M. E.; Williams, D. H.; Cho, Y. R. *Chem. Commun.* **1997**, 1625−1626.

(43) Arriaga, P.; Laynez, J.; Menendez, M.; Canada, J.; Garcia-Blanco, F. *Biochem. J.* **1990**, *265*, 69−77.

(44) Popieniek, P. H.; Pratt, R. F. *J. Am. Chem. Soc.* **1991**, *113*, 2264−2270.

(45) Herrin, T. R.; Thomas, A. M.; Perun, T. J.; Mao, J. C.; Fesik, S. W. *J. Med. Chem.* **1985**, *28*, 1371−1375.

(46) Colombo, L.; Malabarba, A.; Stogniew, M. A61K38/16; A61K31/704; A61P31/04; A61K38/16; A61K31/7028; A61P31/00; US 2009/0305953 A1; Vicuron Pharmaceuticals, Inc.: United States, 2009.

(47) Loll, P. J.; Derhovanessian, A.; Shapovalov, M. V.; Kaplan, J.; Yang, L.; Axelsen, P. H. *J. Mol. Biol.* **2009**, *385*, 200−211.

(48) Nahoum, V.; Spector, S.; Loll, P. J. *Acta Crystallogr. D Biol. Crystallogr.* **2009**, *65*, 832−838.

(49) Groves, P.; Searle, M. S.; Waltho, J. P.; Williams, D. H. *J. Am. Chem. Soc.* **1995**, *117*, 7958−7964.

(50) Loll, P. J.; Bevivino, A. E.; Korty, B. D.; Axelsen, P. H. *J. Am. Chem. Soc.* **1997**, *119*, 1516−1522.

(51) Schafer, M.; Schneider, T. R.; Sheldrick, G. M. *Structure* **1996**, *4*, 1509−1515.

(52) Beauregard, D. A.; Williams, D. H.; Gwynn, M. N.; Knowles, D. J. *Antimicrob. Agents Chemother.* **1995**, *39*, 781−785.

(53) Schafer, M.; Pohl, E.; SchmidtBase, K.; Sheldrick, G. M.; Hermann, R.; Malabarba, A.; Nebuloni, M.; Pelizzi, G. *Helv. Chim. Acta* **1996**, *79*, 1916−1924.

(54) Kaplan, J.; Korty, B. D.; Axelsen, P. H.; Loll, P. J. *J. Med. Chem.* **2001**, *44*, 1837−1840.

(55) Cho, Y. R.; Maguire, A. J.; Try, A. C.; Westwell, M. S.; Groves, P.; Williams, D. H. *Chem. Biol.* **1996**, *3*, 207−215.

(56) Lopez, S.; Hackbarth, C.; Romano, G.; Trias, J.; Jabes, D.; Goldstein, B. P. *J. Antimicrob. Chemother.* **2005**, *55* (Suppl2), ii21−24.

(57) Candiani, G.; Abbondi, M.; Borgonovi, M.; Romano, G.; Parenti, F. *J. Antimicrob. Chemother.* **1999**, *44*, 179−192.

(58) Malabarba, A.; Nicas, T. I.; Ciabatti, R. *Eur. J. Med. Chem.* **1997**, *32*, 459−478.

(59) Malabarba, A.; Ciabatti, R.; Scotti, R.; Goldstein, B. P.; Ferrari, P.; Kurz, M.; Andreini, B. P.; Denaro, M. *J. Antibiot. (Tokyo)* **1995**, *48*, 869−883.

(60) Kantardjieff, K. A.; Rupp, B. *Protein Sci.* **2003**, *12*, 1865−1871.

(61) Mackay, J. P.; Gerhard, U.; Beauregard, D. A.; Maplestone, R. A.; Williams, D. H. *J. Am. Chem. Soc.* **1994**, *116*, 4573−4580.

(62) Loll, P. J.; Axelsen, P. H. *Annu. Rev. Biophys. Biomol. Struct.* **2000**, *29*, 265−289.

(63) Leighton, A.; Gottlieb, A. B.; Dorr, M. B.; Jabes, D.; Mosconi, G.; VanSaders, C.; Mroszczak, E. J.; Campbell, K. C.; Kelly, E. *Antimicrob. Agents Chemother.* **2004**, *48*, 940−945.

(64) Dorr, M. B.; Jabes, D.; Cavaleri, M.; Dowell, J.; Mosconi, G.; Malabarba, A.; White, R. J.; Henkel, T. J. *J. Antimicrob. Chemother.* **2005**, *55* (Suppl 2), ii25−30.

4645

dx.doi.org/10.1021/ja208755j | *J. Am. Chem. Soc.* 2012, 134, 4637−4645